Machine learning predictions of low thermal conductivity: comparing $TaVO_5$ and $GdTaO_4$

Travis Allen*, Jake Graser†, Ramsey Issa‡, Taylor D. Sparks‡§,
* Dept. of Mech. Eng, University of Utah, Salt Lake City, USA
† Northrup Grumman, Salt Lake City, USA
‡ Dept. of Mat. Eng, University of Utah, Salt Lake City, USA
§ Chemistry Department, University of Liverpool, Liverpool, L7 3NY, United Kingdom
Email: § sparks@eng.utah.edu

***Abstract*—Advancements in materials discovery tend to rely disproportionately on happenstance and luck rather than employing a systematic approach. Recently, advances in computational power have allowed researchers to build computer models to predict the material properties of any chemical formula. From energy minimization techniques to machine learning based models, these algorithms have unique strengths and weaknesses. However, a computational model is only as good as its accuracy when compared to real-world measurements. In this work, we take two recommendations from a thermoelectric machine learning model, $TaVO_5$ and $GdTaO_4$, and test their thermoelectric properties of Seebeck coefficient, thermal conductivity, and electrical conductivity. We see that the predictions are mixed; thermal conductivities are correctly predicted, while electrical conductivities and Seebeck coefficients are not. Furthermore, we discover a possible new avenue of research of a low thermal conductivity oxide family.**

***Index Terms*—thermoelectrics, oxides, data-driven, materials informatics, thermal conductivity, NTE**

I. Introduction

Accelerating worldwide energy demand and interest in preventative measures regarding global climate change have led to increasing development of diverse methods of energy production. One such method is the use of thermoelectric generators to capture waste heat [1]. Thermoelectric generators rely on thermoelectric materials, which can generate an electric potential difference (i.e. a voltage) from a temperature gradient with with no moving parts. This unique set of properties makes these materials promising for a wide variety of engineering applications. However, current thermoelectric devices suffer from low efficiency and often rely on rare and expensive elements, so they have thus far been relegated to use in mission critical applications where no other options are available, such as space applications including rovers and probes. [2]–[5]. Indeed, some of the highest performance thermoelectric materials utilize toxic elements, such as PbTe, making them unfit for many uses. New high-efficiency and low-cost thermoelectric materials will need to be discovered to enable broader device applications.

Unfortunately, discovering new high-efficiency materials has proven challenging. Device efficiency scales with zT, which can be calculated using the relation

$$zT = \frac{S^2\sigma}{\kappa}T \tag{1}$$

where S is the Seebeck coefficient, σ is electrical conductivity, κ is thermal conductivity, and T is temperature. From this we can see that the ideal thermoelectric is electrically conductive but thermally resistive. The challenge is that these properties are interrelated, making the maximization of zT non-trivial. Many strategies have been developed for maximizing electrical transport while minimizing thermal transport, and previous work has shown that some chemical systems have reached the point of diminishing returns in enhancing zT through thermal conductivity reduction, while others have not [1], [6].

The large potential compositional and structural space available for exploration makes this challenge perhaps well-suited for data-driven approaches. In recent years, materials informatics, or data science tools directed towards materials research, have proven valuable in the rapid discovery and development of a variety of different materials including photovoltaics, superhard materials, metal alloys, and more [7]–[9]. In the field of thermoelectrics itself materials informatics is finding increasing application [10]–[12]. A recent report used machine learning models to identify a new aperiodic structure transition metal oxide, $Ba_{10}Y_6Ti_4O_{27}$, with thermal conductivity among the lowest ever measured for an oxide [13]. In this paper, we evaluate two new oxides, $TaVO_5$ and $GdTaO_4$, as candidates for low thermal conductivity materials and measure their thermoelectric properties, relating the observed transport to their structures.

II. Materials and Methods

A. Machine Learning Algorithm

The machine learning model used to make materials recommendations was described previously [12]. Briefly, a random forest algorithm was trained on a combined dataset created using experimental data taken from literature values, the NIMS database, and the Materials Project. Rather than predicting materials properties via regression, the model instead treated predictions as classifications of whether or not they would have values above or below a given cut-off. For a given chemical formula, the model assigns a confidence value with a score p, where $p \in (0, 1)$, for four physical properties that correlate with desired thermoelectric behavior. The score represents the probability that the property meets the specified cutoffs defined for the absolute Seebeck coefficient ($S > 100\,\mu V{\cdot}K^{-1}$),

electrical conductivity ($\sigma < 10^{-2}\,\Omega{\cdot}$cm), thermal conductivity ($\kappa < 10\,\mathrm{W{\cdot}m^{-1}{\cdot}K^{-1}}$) and band gap ($E_g > 0\,$eV).

B. Synthesis of $TaVO_5$

In accordance with Wang et al. [14], stoichiometric powders of Ta_2O_5 and V_2O_5 were mixed with ethanol and ball milled for ten hours with zirconia media. This mixture was then allowed to dry overnight. The dried powder mixture was then ground with an agate mortar and pestle and pressed into 13 mm diameter discs. These were buried in sacrificial powder and underwent reaction heating at 800°C for 24 hours. Sacrificial powder was used to reduce vanadium loss during synthesis as vanadium would diffuse into the alumina crucible boats during reaction heating. The discs were then crushed into powder with an agate mortar and pestle, and the powder was spark plasma sintered at California Nanotechnologies Inc. under a load of 5.7 kN for 20 minutes at 1000°C to achieve maximum density for thermal and electrical measurements.

C. Synthesis of $GdTaO_4$

In accordance with Yang et. al. [15], $GdTaO_4$ was synthesized with starting materials Gd_2O_3 and Ta_2O_5, which were calcined at 800°C for 8 hours. Stoichiometric powders of these calcined starting materials were mixed with ethanol and ball milled for ten hours with zirconia media. This mixture was allowed to dry overnight. The dried powder mixture was then ground with an agate mortar and pestle and pressed into 13 mm diameter discs. These discs underwent reaction heating at 1400°C for 12 hours. The discs were then crushed into powder with an agate mortar and pestle, and the resulting powder was spark plasma sintered at California Nanotechnologies Inc. under a load of 5.7 kN for 29 minutes at 1500°C to achieve maximum density for thermal and electrical measurements.

D. Material Characterization

Powder X-ray diffraction measurements were taken with a Bruker D2 Phaser diffractometer. Quantitative phase analysis was carried out by the Rietveld refinement method using GSAS-II software [16]. Heat capacity measurements were taken on small portions of the synthesized powder using a Netzsch 3500 DSC differential scanning calorimeter.

The sintered discs were mounted in epoxy and cut with a diamond saw to a thickness of one to two millimeters for the measurement of the Seebeck coefficient, electrical conductivity, and thermal diffusivity. Prior to measurement, discs were sanded with a 1200 grit sandpaper on a Struers TegraPol-11. The electrical conductivity and Seebeck coefficient were measured using a Netzsch Nemesis 458 which has a 7% standard error for Seebeck coefficient and a 5% standard error for electrical conductivity. The thermal diffusivity was measured via the laser flash technique on a Netzsch LFA 457, which has a standard error of 10%. The bulk density was measured with the Archimedes method in an immersion medium of deionized water. Thermal conductivity was calculated using the standard relationship:

$$\kappa = \alpha C_p \rho \tag{2}$$

where α is thermal diffusivity, C_p is heat capacity, and ρ is bulk density.

III. Results

X-ray diffraction spectra for the $TaVO_5$ sample along with Rietveld refinement are shown in Figure 1. A good fit, R_{wp}=9.85%, was obtained by including two phases, $TaVO_5$ and Ta_2O_5, in the refinement. $TaVO_5$ was shown to be approximately 98% pure with approximately 2wt% Ta_2O_5 impurities. Meanwhile, X-ray diffraction spectra for the $GdTaO_4$ sample along with Rietveld refinement are shown in Figure 2. A similarly good fit, R_{wp}=8.68%, was obtained by including two phases, $GdTaO_4$ and Gd_2O_3, in the refinement. $GdTaO_4$ was shown to be approximately 95% pure with approximately 5wt% Gd_2O_3 impurities.

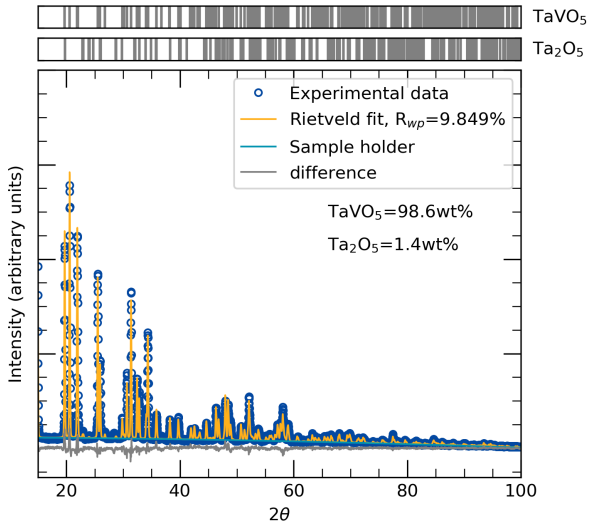

Fig. 1. Rietveld refinement of powder X-ray diffraction data from $TaVO_5$ samples showing a high purity sample with <2wt% Ta_2O_5 impurity.

Since this study was focused specifically on machine learning predictions of thermal conductivity, stoichiometric oxides of both $TaVO_5$ and $GdTaO_4$ were synthesized. By simple electron counting one would rightly predict both Ta[V]V[V]O_5 and Gd[III]Ta[V]O_4 to be insulators, and this was confirmed by electrical conductivity measurements which were all outside the bounds of the Nemesis 458, signifying a conductivity below the limitations of $0.05\,\mathrm{S{\cdot}cm^{-1}}$. Density functional theory (DFT) calculations from literature suggest $TaVO_5$ to have an indirect band gap of 2.11 eV [17], and $GdTaO_4$ to have an indirect band gap of 4.86 eV [18].

Thermal conductivity measurements, shown in Figures 3 and 4, confirm the predictions that $TaVO_5$ is a very low thermal conductivity material, particularly among oxides, while $GdTaO_4$ is not. The thermal conductivity of $TaVO_5$ is both low and nearly independent of temperature. $TaVO_5$ reaches a maximum value of $1.34\,\mathrm{W{\cdot}m^{-1}{\cdot}K^{-1}}$ at 100°C and then drops consistently until reaching a minimum thermal conductivity of $1.2\,\mathrm{W{\cdot}m^{-1}{\cdot}K^{-1}}$, well below the machine learning threshold cutoff value of $10\,\mathrm{W{\cdot}m^{-1}{\cdot}K^{-1}}$. $GdTaO_4$, on the other

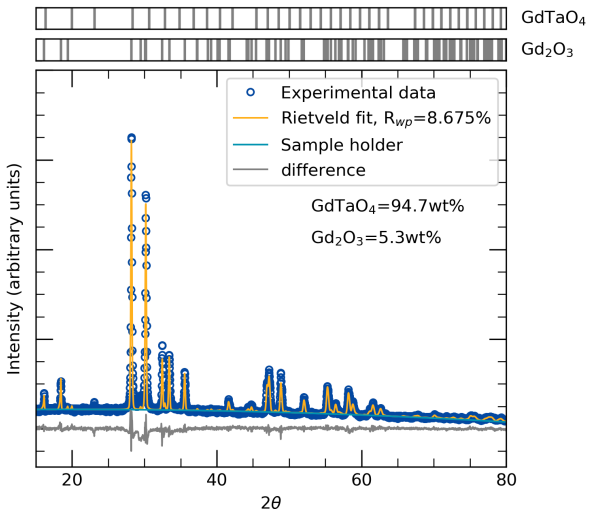

Fig. 2. Rietveld refinement of powder X-ray diffraction data from $GdTaO_4$ samples showing a high purity sample with approximately 5wt% Gd_2O_3 impurity.

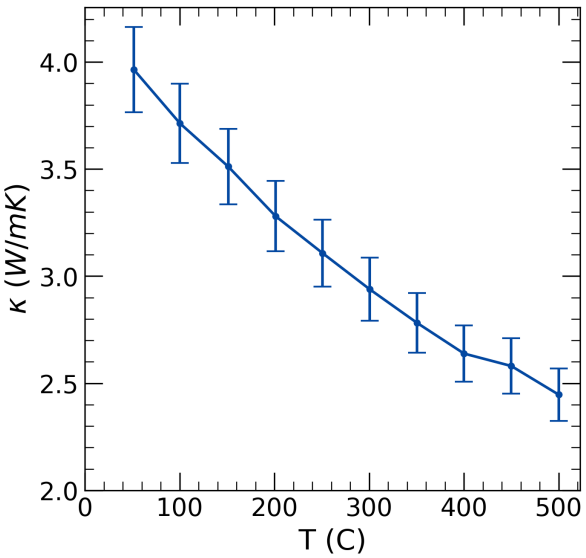

Fig. 4. Thermal conductivity of $GdTaO_4$ during heating.

hand, has a thermal conductivity of $4\,\mathrm{W{\cdot}m^{-1}{\cdot}K^{-1}}$ at room temperature and the typical 1/T temperature dependence as it approaches the value of $2.5\,\mathrm{W{\cdot}m^{-1}{\cdot}K^{-1}}$ at 500°C.

In $TaVO_5$ we observed during initial laser flash measurements that at higher temperatures, vanadium loss became apparent with $TaVO_5$ decomposing into Ta_9VO_{25}. Therefore, samples were only measured up to 500°C in order to maintain $TaVO_5$ phase stability. Samples measured at higher temperatures had large hysteresis between heating and cooling which we attribute to vanadium volatilization. New samples were synthesized and laser flash measurements were taken up to 500°C to avoid volatilization and hysteresis.

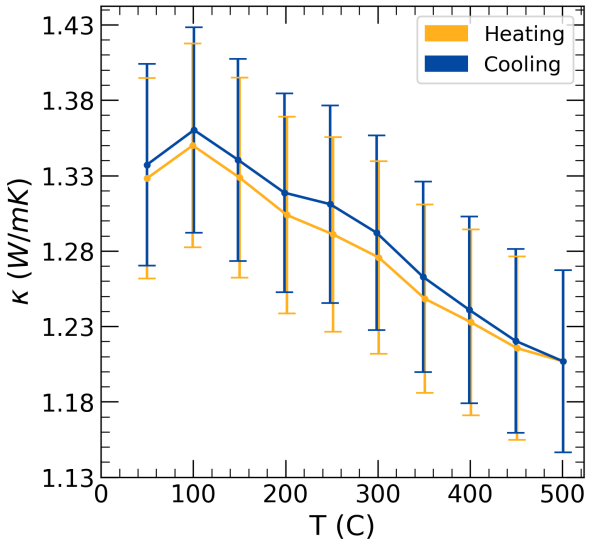

Fig. 3. Thermal conductivity of $TaVO_5$. Orange is thermal conductivity during heating while blue is during cooling.

IV. Discussion

Given the low electrical conductivity of both $TaVO_5$ and $GdTaO_4$, the electrical contributions to the overall thermal conductivities were calculated to be negligible. $TaVO_5$ ranks lower than many well-known low thermal conductivity oxides as outlined by Winter et al. [19]. This is noteworthy considering that most low thermal conductivity oxides achieve low lattice thermal conductivities by relying on phonon scattering due to aliovalent doping producing vacancies on the cation or anion sublattices [20], [21].

Why is the thermal conductivity of $TaVO_5$ so much lower than that of $GdTaO_4$? There are several possible factors that could be responsible. Let us first consider the Debye temperature, θ_D. Previous work has shown that θ_D, the temperature of a crystal's highest normal mode of vibration, correlates with structural rigidity and thus has implications regarding a crystal's thermal properties [22]. While the Debye temperature can difficult to measure in practice, it can be calculated using elastic constants with the following relation:

$$\theta_D = \frac{h}{k_\mathrm{B}}\left[\frac{3n}{4\pi}\left(\frac{N_\mathrm{A}\rho}{M}\right)\right]^{1/3} v_m \tag{3}$$

where h and k_B have their usual meanings, n is the number of atoms per formula unit, N_A is Avogadro's number, ρ is the density of the crystal structure, M is molar mass, and v_m is the mean sound speed [23]. The mean sound speed for a polycrystalline material can be approximated with the relation:

$$v_m = \left[\frac{1}{3}\left(\frac{2}{v_T^3} + \frac{1}{v_L^3}\right)\right]^{-1/3} \tag{4}$$

where v_T is the transverse sound speed and v_L is the longitudinal sound speed. These can be obtained from the bulk and

shear moduli [24]:

$$v_T = \left(\frac{G}{\rho}\right)^{1/2} \tag{5}$$

$$v_L = \left(\frac{B + \frac{4G}{3}}{\rho}\right)^{1/2} \tag{6}$$

Bulk and shear moduli values of 65 GPa and 140 GPa, respectively, were previously calculated for $GdTaO_4$ via density functional theory (DFT) [25]. Elastic constants for $TaVO_5$ were unavailable in the literature so they were instead estimated using a machine learning model developed by our group and described in a previous publication [26]. The details including code and data are in Wang et al's original publication, but briefly, we summarize the method here. To estimate the bulk and shear moduli, materials Project data was curated via the Materials Project python API `MPRester`. Data for training the compositionally restricted attention-based network (`CrabNet`) model was extracted using three key fields; the chemical formula from the field `'formula_pretty'`, and the Voigt-Reuss-Hill average bulk and shear moduli from the fields `'k_vrh'` and `'g_vrh'`. The extraction of the data resulted in a DataFrame that contained 154,718 formulae. We then preprocessed the data, removing formulas for which `'k_vrh'` and `'g_vrh'` had not been calculated using DFT. The removal of cells containing `NaN` in either column (`'k_vrh'` and `'g_vrh'`) was done separately for each elastic constant to ensure removal of cells that might have had only one value calculated. Next, we removed any formula which matched our target formula ($TaVO_5$) to ensure no data leakage when making a prediction using our models. The preprocessing steps resulted in 7,107 training points for each model to train on. The `CrabNet` model internally scales and standardizes the input data, so this step was handled automatically. We then separately trained two models, one on `'k_vrh'` and another on `'g_vrh'`. Both models had a batch-size of 256 and were trained for 100 epochs. Each `CrabNet` model had 512 embedding dimensions and three layers, each with 4 parallel attention mechanisms. These predictions resulted in bulk and shear moduli of 49.7$\pm$11.0 GPa and 156$\pm$15.1 GPa, respectively. Using these values, we report estimated Debye temperatures of 459 K for $TaVO_5$ and 406 K for $GdTaO_4$. It must be noted that higher accuracy estimates of the Debye temperature would come from calculations made with measured elastic constants or entirely DFT-calculated elastic constants.

While the two estimated Debye temperatures are quite close, the Debye temperature of $TaVO_5$ exceeds that of $GdTaO_5$. This is unexpected given that the thermal conductivity of $TaVO_5$ is considerably lower than that of $GdTaO_4$. However, the Debye temperature is not the only material property that influences thermal conductivity. Other metrics, such as mass contrast and polyhedral connectivity of the crystal structure itself, can also dictate thermal conductivity.

Let us first consider atomic mass. It is known that large atomic mass atoms, such as Ta, and compounds with large mass contrast between atoms result in lower thermal conductivity [20], [27], [28]. If we assume a Debye phonon spectrum, the thermal conductivity is dependent on the inverse square root of the defect phonon scattering coefficient at temperatures above the Debye temperature:

$$\kappa \propto \Gamma^{-1/2} \tag{7}$$

where

$$\Gamma_i = x_i \left[\left(\frac{M_i - \overline{M}}{\overline{M}} \right)^2 + \epsilon \left(\frac{\delta_i - \overline{\delta}}{\overline{\delta}} \right)^2 \right] \tag{8}$$

for the ith defect, where x_i is the concentration of the defect, M_i is the mass of the defect, δ_i is the atomic size of the defect, $\overline{M}$ is the average mass, and $\overline{\delta}$ is the average atomic size. This implies that the scattering coefficient depends on the concentration of defects, their size contrast, $\Delta\delta^2 = (\delta_i - \overline{\delta})^2$, and their mass contrast, $\Delta M^2 = (M_i - \overline{M})^2$. We don't explicitly consider the size contrast as we lack sufficient information regarding the effective size of ions and vacancies to make any rigorous claims about the effect of size contrast on the scattering coefficient. Nevertheless, we can easily observe that the mass contrast of $TaVO_5$ is substantially higher than it is for $GdTaO_4$. This implies that $TaVO_5$ has a larger scattering coefficient and thus a lower thermal conductivity than does $GdTaO_4$, which our experiments confirm. However, this cannot alone explain the low thermal conductivity in $TaVO_5$. For example, consider Ta_2O_5 which exhibits both of these qualities (high atomic mass atoms, large mass contrast) but has a thermal conductivity over three times that of $TaVO_5$ in defect-free films [29].

The low thermal conductivity is likely intrinsically related to the crystal structure of $TaVO_5$ itself. As seen in Figure 5, the TaO_6 octahedra is only corner-shared with the VO_4 polyhedra. This flexible linkage implies that the structure is more likely to twist and change volume during acoustic phonon propagation, lowering its thermal conductivity [19], [20]. Additionally, the large mass contrast between vanadium and tantalum within the lattice is likely to cause phonon dampening, limit the phonon's degrees of freedom, and interrupt the possible phonon modes [21]. This determination is further supported by previous Raman scattering measurements showing limited vibrational nodes as well as distortion of octahedra and polyhedra at higher temperatures [6].

$TaVO_5$ and other comparable oxides in the same *Pnma* space group, such as $NbVO_5$ and $TaPO_5$, are negative thermal expansion (NTE) materials [30]–[32]. This is unsurprising as the same anharmonicity of low-frequency phonon modes that gives rise to NTE also results in the coupled phonons and shorter mean free path lengths that are typically associated with low thermal conductivity [33]. Literature review shows a gap of thermal conductivity predictions and measurements for this family of oxides. These *Pnma* corner-shared oxides, such as $NbVO_5$ and $TaPO_5$, could represent a new avenue of low thermal conductivity materials that have yet to be fully explored.

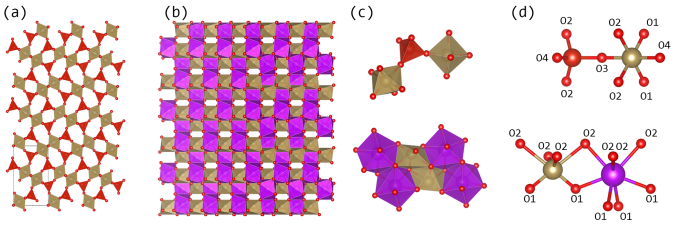

Fig. 5. Extended crystal structure views of (a) $TaVO_5$ and (b) $GdTaO_4$ and local polyhedral connectivity diagrams (c) and atomic labels (d).

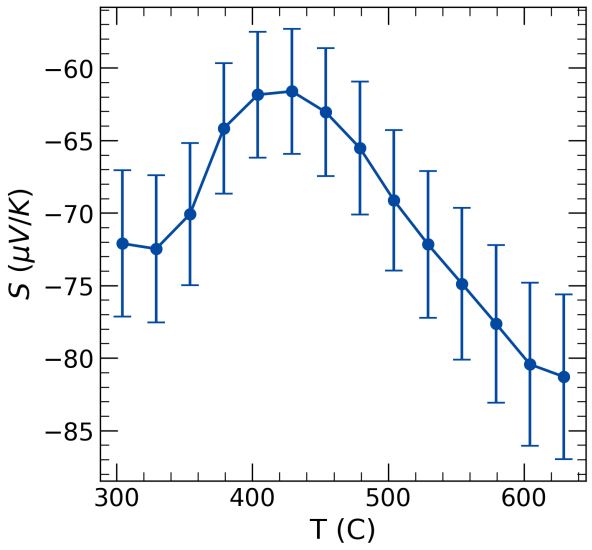

Fig. 6. Seebeck coefficient of $TaVO_5$.

Seebeck coefficient, as seen as Figure 6, was measured to be around -70 $\pm$ 10 $\mu V \cdot K^{-1}$ within the range of 300°C to 600°C before vanadium loss became an issue. $TaVO_5$ lower Seebeck coefficient can be explained by using the density functional theory calculations of band structure which suggest that $TaVO_5$ has a broad band structure leading to low effective mass for electrons in the conduction band [14]. This makes $TaVO_5$ an improbable thermoelectric since improving the low electrical conductivity would require heavy doping which, following Mott's formula and the Wiedemann-Franz law, would further decrease the Seebeck coefficient [1], [34].

The electrical conductivity of $GdTaO_4$ was unmeasurable on the Nemesis 458, suggesting its conductivity to be somewhere below the limitations of 0.05 $S \cdot cm^{-1}$. Further measurements done at room temperature with a Keithley 2000 multimeter showed the resistance above the limitations of the machine at 120 MΩ. This is likely due to the oxide following the completed shell of 18 electron rule, as well as having a large band gap, requiring a noticeable energy to excite electrons into the valence band.

Thermal conductivity, as shown in Figure 4, was shown to start at 4 $W \cdot m^{-1} \cdot K^{-1}$ and steadily decrease to 2.5 $W \cdot m^{-1} \cdot K^{-1}$ at the 500°C upper bound of our differential scanning calorimeter. This is on par with literature from single crystal and polycrystal measurements [15], [35]–[37].

The higher than expected thermal conductivity of $GdTaO_4$ can be explained by having a more interconnected crystal structure as well as the similar atomic weights of gadolinium and tantalum. This allows more phonon modes to exist within the structure. Single crystal studies support this theory, showing similar sloping decreases in thermal conductivity as well as low thermal anisotropy [15]. Despite the fact that this is well below the cutoff value of 10 $W \cdot m^{-1} \cdot K^{-1}$ given by the machine learning algorithm, $GdTaO_4$ seems questionable as a thermoelectric material without a noticeable decrease in the higher temperature ranges when compared to known thermoelectric systems of interest, which reside below 1 $W \cdot m^{-1} \cdot K^{-1}$ before doping [6], [34].

The Seebeck coefficient measurements of $GdTaO_4$ showed large variation and lack of continuity and are thus not reported. The large amount of noise and lack of linearity in the measurement suggests that the Seebeck coefficient is far below the limitations of the Nemesis 458 of 10 $\mu V \cdot K^{-1}$. $GdTaO_4$ shows a shallow band structure as seen in Ding et al. [18], Materials Project [38], and Topological Materials Database [35]–[37] which suggest low effective masses for both carriers.

It should be noted that these sources have similar shallow band structures but show contradictions for band gap. The Topological Materials Database [35]–[37] lists $GdTaO_4$ as a semimetal while others such as the Materials Project [38] and Ding et al. [18] suggest a large band gap ranging from 3.26 eV to 4.86 eV respectively. Our electrical conductivity measurements support the notion that this material is a wide-gap semiconductor and is not a semimetal. Curvature of the band structure indicates similar effective masses for both carriers. This in conjunction with a large band gap means the bipolar effect further constrains the magnitude of the Seebeck coefficient [15].

By using predictions to excite and motivate scientists, machine learning gives us a promising direction to explore chemical whitespace. However, these tools are very dependent on training data as well as algorithm choice and as such require scrutiny and verification. In the case of the Citrination engine model, we chose two of the recommended oxide compounds to test as thermoelectric materials: $TaVO_5$ and $GdTaO_4$. It was shown that for predicting thermal conductivity, the model preformed as expected with both compounds being well below the cutoff of 10 $W \cdot m^{-1} \cdot K^{-1}$. However other predictions such as electrical conductivity and Seebeck coefficient were incorrect, making the model an imperfect tool. Nevertheless, the pursuit of data driven research has pointed us to the possibility of a new family of low thermal conductivity oxides which require further study. These physical measurements will also allow thermoelectric-based machine learning algorithms to grow and be refined for even stronger recommendations in the future.

ACKNOWLEDGMENTS

The authors gratefully acknowledge funding and support from the National Science Foundation through award NSF DMR 1651668. Special thanks to Clayton Cozzan and Dr. Ram Seshadri for preliminary assistance in sintering trial runs prior to final synthesis. We would like to thank Eric Eyerman at California Nanotechnologies Inc. for his assistance.

DISCLOSURES

The authors report there are no competing interests to declare.

REFERENCES

[1] G. J. Snyder and E. S. Toberer, "Complex thermoelectric materials," *Nature materials*, vol. 7, no. 2, pp. 105–114, 2008.

[2] L. Jones, V. Moreno, and R. Zimmerman, "The f1 multi-mission radioisotope thermoelectric generator (mmrtg): A power subsystem enabler for the mars science laboratory (msl) mission," 2013.

[3] M. W. Gaultois, T. D. Sparks, C. K. Borg, R. Seshadri, W. D. Bonificio, and D. R. Clarke, "Data-driven review of thermoelectric materials: performance and resource considerations," *Chemistry of Materials*, vol. 25, no. 15, pp. 2911–2920, 2013.

[4] G. Haxel, *Rare earth elements: critical resources for high technology*. US Department of the Interior, US Geological Survey, 2002, vol. 87, no. 2.

[5] U. DoE, "Critical materials strategy 2011," *Washington, DC: United State s Department of Energy*, 2011.

[6] M. W. Gaultois and T. D. Sparks, "How much improvement in thermoelectric performance can come from reducing thermal conductivity?" *Applied Physics Letters*, vol. 104, no. 11, p. 113906, 2014.

[7] B. Cao, L. A. Adutwum, A. O. Oliynyk, E. J. Luber, B. C. Olsen, A. Mar, and J. M. Buriak, "How to optimize materials and devices via design of experiments and machine learning: Demonstration using organic photovoltaics," *ACS nano*, vol. 12, no. 8, pp. 7434–7444, 2018.

[8] A. Mansouri Tehrani, A. O. Oliynyk, M. Parry, Z. Rizvi, S. Couper, F. Lin, L. Miyagi, T. D. Sparks, and J. Brgoch, "Machine learning directed search for ultraincompressible, superhard materials," *Journal of the American Chemical Society*, vol. 140, no. 31, pp. 9844–9853, 2018.

[9] J. H. Martin, B. D. Yahata, J. M. Hundley, J. A. Mayer, T. A. Schaedler, and T. M. Pollock, "3d printing of high-strength aluminium alloys," *Nature*, vol. 549, no. 7672, pp. 365–369, 2017.

[10] J. Carrete, W. Li, N. Mingo, S. Wang, and S. Curtarolo, "Finding unprecedentedly low-thermal-conductivity half-heusler semiconductors via high-throughput materials modeling," *Physical Review X*, vol. 4, no. 1, p. 011019, 2014.

[11] T. D. Sparks, M. W. Gaultois, A. Oliynyk, J. Brgoch, and B. Meredig, "Data mining our way to the next generation of thermoelectrics," *Scripta Materialia*, vol. 111, pp. 10–15, 2016.

[12] M. W. Gaultois, A. O. Oliynyk, A. Mar, T. D. Sparks, G. J. Mulholland, and B. Meredig, "Perspective: Web-based machine learning models for real-time screening of thermoelectric materials properties," *Apl Materials*, vol. 4, no. 5, p. 053213, 2016.

[13] C. M. Collins, L. M. Daniels, Q. Gibson, M. W. Gaultois, M. Moran, R. Feetham, M. J. Pitcher, M. S. Dyer, C. Delacotte, M. Zanella *et al.*, "Discovery of a low thermal conductivity oxide guided by probe structure prediction and machine learning," *Angewandte Chemie International Edition*, vol. 60, no. 30, pp. 16 457–16 465, 2021.

[14] X. Wang, Q. Huang, J. Deng, R. Yu, J. Chen, and X. Xing, "Phase transformation and negative thermal expansion in tavo5," *Inorganic chemistry*, vol. 50, no. 6, pp. 2685–2690, 2011.

[15] H. Yang, F. Peng, Q. Zhang, C. Guo, C. Shi, W. Liu, G. Sun, Y. Zhao, D. Zhang, D. Sun *et al.*, "A promising high-density scintillator of gdtao 4 single crystal," *CrystEngComm*, vol. 16, no. 12, pp. 2480–2485, 2014.

[16] B. H. Toby and R. B. Von Dreele, "Gsas-ii: the genesis of a modern open-source all purpose crystallography software package," *Journal of Applied Crystallography*, vol. 46, no. 2, pp. 544–549, 2013.

[17] R. Kontic, "New pathways to oxide materials for photocatalytic applications," Ph.D. dissertation, University of Zurich, 2014.

[18] S. Ding, A. Kinross, X. Wang, H. Yang, Q. Zhang, W. Liu, and D. Sun, "Experiment and density functional theory analyses of gdtao4 single crystal," *Solid State Communications*, vol. 273, pp. 5–10, 2018.

[19] M. R. Winter and D. R. Clarke, "Oxide materials with low thermal conductivity," *Journal of the American Ceramic Society*, vol. 90, no. 2, pp. 533–540, 2007.

[20] Z. Qu, T. D. Sparks, W. Pan, and D. R. Clarke, "Thermal conductivity of the gadolinium calcium silicate apatites: Effect of different point defect types," *Acta Materialia*, vol. 59, no. 10, pp. 3841–3850, 2011.

[21] W. Pan, S. R. Phillpot, C. Wan, A. Chernatynskiy, and Z. Qu, "Low thermal conductivity oxides," *Mrs Bulletin*, vol. 37, no. 10, pp. 917–922, 2012.

[22] J. Brgoch, S. P. DenBaars, and R. Seshadri, "Proxies from ab initio calculations for screening efficient ce3+ phosphor hosts," *The Journal of Physical Chemistry C*, vol. 117, no. 35, pp. 17 955–17 959, 2013.

[23] O. L. Anderson, "A simplified method for calculating the debye temperature from elastic constants," *Journal of Physics and Chemistry of Solids*, vol. 24, no. 7, pp. 909–917, 1963.

[24] Y. Zhuo, A. Mansouri Tehrani, A. O. Oliynyk, A. C. Duke, and J. Brgoch, "Identifying an efficient, thermally robust inorganic phosphor host via machine learning," *Nature communications*, vol. 9, no. 1, pp. 1–10, 2018.

[25] M. De Jong, W. Chen, T. Angsten, A. Jain, R. Notestine, A. Gamst, M. Sluiter, C. Krishna Ande, S. Van Der Zwaag, J. J. Plata *et al.*, "Charting the complete elastic properties of inorganic crystalline compounds," *Scientific data*, vol. 2, no. 1, pp. 1–13, 2015.

[26] A. Y.-T. Wang, S. K. Kauwe, R. J. Murdock, and T. D. Sparks, "Compositionally restricted attention-based network for materials property predictions," *Npj Computational Materials*, vol. 7, no. 1, pp. 1–10, 2021.

[27] F. J. DiSalvo, "Thermoelectric cooling and power generation," *Science*, vol. 285, no. 5428, pp. 703–706, 1999.

[28] E. S. Toberer, L. L. Baranowski, and C. Dames, "Advances in thermal conductivity," *Annual Review of Materials Research*, vol. 42, no. 1, pp. 179–209, 2012.

[29] C. D. Landon, R. H. Wilke, M. T. Brumbach, G. L. Brennecka, M. Blea-Kirby, J. F. Ihlefeld, M. J. Marinella, and T. E. Beechem, "Thermal transport in tantalum oxide films for memristive applications," *Applied Physics Letters*, vol. 107, no. 2, p. 023108, 2015.

[30] J. Wang, J. Deng, R. Yu, J. Chen, and X. Xing, "Coprecipitation synthesis and negative thermal expansion of nbvo 5," *Dalton Transactions*, vol. 40, no. 13, pp. 3394–3397, 2011.

[31] T. G. Amos, *Negative thermal expansion in AOMO (4) compounds*. Oregon State University, 2000.

[32] N. Shi, Y. Song, X. Xing, and J. Chen, "Negative thermal expansion in framework structure materials," *Coordination Chemistry Reviews*, vol. 449, p. 214204, 2021.

[33] C. A. Kennedy and M. A. White, "Unusual thermal conductivity of the negative thermal expansion material, zrw2o8," *Solid state communications*, vol. 134, no. 4, pp. 271–276, 2005.

[34] A. Zevalkink, D. M. Smiadak, J. L. Blackburn, A. J. Ferguson, M. L. Chabinyc, O. Delaire, J. Wang, K. Kovnir, J. Martin, L. T. Schelhas *et al.*, "A practical field guide to thermoelectrics: Fundamentals, synthesis, and characterization," *Applied Physics Reviews*, vol. 5, no. 2, p. 021303, 2018.

[35] B. Bradlyn, L. Elcoro, J. Cano, M. G. Vergniory, Z. Wang, C. Felser, M. I. Aroyo, and B. A. Bernevig, "Topological quantum chemistry," *Nature*, vol. 547, no. 7663, pp. 298–305, 2017.

[36] M. Vergniory, L. Elcoro, C. Felser, N. Regnault, B. A. Bernevig, and Z. Wang, "A complete catalogue of high-quality topological materials," *Nature*, vol. 566, no. 7745, pp. 480–485, 2019.

[37] M. G. Vergniory, B. J. Wieder, L. Elcoro, S. S. Parkin, C. Felser, B. A. Bernevig, and N. Regnault, "All topological bands of all nonmagnetic stoichiometric materials," *Science*, vol. 376, no. 6595, p. eabg9094, 2022.

[38] A. Jain, S. P. Ong, G. Hautier, W. Chen, W. D. Richards, S. Dacek, S. Cholia, D. Gunter, D. Skinner, G. Ceder *et al.*, "Commentary: The materials project: A materials genome approach to accelerating materials innovation," *APL materials*, vol. 1, no. 1, p. 011002, 2013.